Application of an energy-dependent instrument response function to analysis of nTOF data from cryogenic DT experiments

Z. L. Mohamed,[a] O. M. Mannion, J. P. Knauer, C. J. Forrest, V. Yu. Glebov, C. Stoeckl, and M. H. Romanofsky
Laboratory for Laser Energetics, University of Rochester, Rochester, NY 14623 USA

Neutron time-of-flight (nTOF) detectors are used to diagnose the conditions present in inertial confinement fusion (ICF) experiments and basic laboratory physics experiments performed on an ICF platform. The instrument response function (IRF) of these detectors is constructed by convolution of two components: an x-ray IRF and a neutron interaction response. The shape of the neutron interaction response varies with incident neutron energy, changing the shape of the total IRF. Analyses of nTOF data that span a broad range of energies must account for this energy-dependence in order to accurately infer plasma parameters and nuclear properties in ICF experiments. This work briefly reviews a matrix multiplication approach to convolution which allows for an energy-dependent change in the shape of the IRF. This method is applied to synthetic data resembling symmetric cryogenic DT implosions to examine the effect of the energy-dependent IRF on the inferred areal density. Results of forward fits that infer ion temperatures and areal densities from nTOF data collected during cryogenic DT experiments on OMEGA are also discussed.

I. INTRODUCTION

Areal density is a quantity that is used to diagnose the compressive performance of cryogenic DT inertial confinement fusion (ICF) experiments. With the recent development of a second xylene neutron time-of-flight (nTOF) line of sight (LOS) on OMEGA that uses the same detector design as an existing OMEGA nTOF,[1–3] an additional measurement of backscatter areal density is now available, enabling more detailed study of implosion symmetry via variations in areal density. This work briefly details the design of the two xylene nTOF's on OMEGA as well as the analysis that is used to infer backscatter areal density.

Recent developments on the analysis of nTOF data at OMEGA include analysis over a larger range of energies (1.5 to 4 MeV) in order to properly characterize the background as well as the spectrum of backscattered neutrons. Accurate analysis over this extended range of energies requires the use of an energy-dependent instrument response function (IRF). In general, the total IRF is constructed by convolving a measured x-ray IRF with a neutron interaction response that can be calculated using a particle transport code such as MCNP.[4] Neutrons of different energies have different transit times across the detector and deposit different levels of energy in the detector material, so the shape of the neutron interaction response is energy-dependent. This causes energy-dependence in the shape of the total IRF. The convolution operation can be represented as multiplication with a Toeplitz matrix. Convolution with an energy-dependent IRF can be therefore be represented as matrix multiplication with a modified Toeplitz matrix in which each column of the matrix represents a monoenergetic IRF of a different energy. Further mathematical details of this method can be found in Ref. 5.

This forward fit analysis of the areal density has been benchmarked using synthetic data representing symmetric, isobaric implosions that were generated using the particle tracking code *IRIS3D*.[6] This method has been applied to a set of experimental data dating back to early 2019, when the second xylene nTOF LOS came online.

II. DETECTOR DESIGN AND LINES OF SIGHT

Both of the OMEGA nTOF detectors that are used to infer areal density from backscattered neutrons are liquid xylene detectors. Xylene is used as a scintillator while photomultiplier tubes (PMT's) are used as photodetectors. The two detectors have an identical design that is detailed in Ref. 2 and Ref. 3. Each detector consists of a 20-cm-diam. × 10-cm-thick cylindrical volume of xylene that is contained within a stainless-steel housing. There are four windows along the edges of the housing, located equidistant from one another. A gated PMT is placed on each of these windows for detection of the scintillation light that is produced when energy is deposited in the xylene. The use of four gated PMT's allows for measurement of the signal over a large dynamic range.[1,2] This large dynamic range enables measurement of the high-energy (14.03-MeV), high-yield ($\sim 1 \times 10^{14}$) DT neutrons in addition to the low-energy DD (2.45-MeV) and backscattered DT (3- to 4-MeV) neutrons, which typically have a yield in the 1×10^{10} to 1×10^{11} range during cryogenic DT implosions. The areal density measurement depends upon measurement of the backscattered DT neutrons as well as the primary DT yield, although primary DT yield is also measured by several other detectors on OMEGA.

Since it is known that the light output of xylene changes as the liquid ages and its oxygen level decreases,[7] the xylene used in both detectors is replaced with freshly oxygenated xylene every three months on OMEGA. Detector calibration is performed on each cryogenic shot day using two DD implosions that precede cryogenic DT

[a] zmoh@lle.rochester.edu

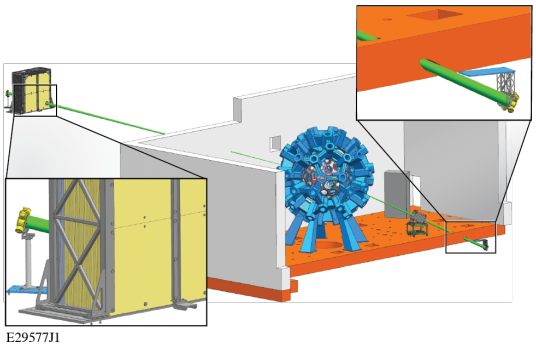

FIG. 1. Schematic showing the two nTOF LOS. The additional panels show magnified views of the detectors at the end of the LOS. The green cones show each detector's LOS to TCC.

implosions. Calibration is carried out by calculating the charge detected by a given PMT in response to DD neutrons. This charge along with a standard measurement of DD neutron yield from another detector can then be used to calculate a charge per neutron at ∼2.45 MeV (i.e., a calibration constant).[3] The standard DD yield for this calibration comes from a separate detector which has been cross-calibrated to indium activation measurements and consists of a 40-mm-diam × 20-mm-thick plastic scintillator coupled to a two-stage MCP PMT.[8] Once the calibration constant at 2.45 MeV has been calculated, it can be scaled by the detector sensitivity and beamline attenuation — both functions of incident neutron energy — to determine the charge per neutron at other neutron energies.[9]

Each of the detectors is located along a collimated line of sight. The relative positions of the two detectors are shown in Fig. 1. The original xylene detector is located 13.4 m from target chamber center (TCC), below the level of the OMEGA Target Bay. A concrete floor is located between the detector and the OMEGA Target Bay, with a hole bored diagonally through the concrete to give the detector a clear line of sight to the target chamber. Within the Target Bay, additional collimation is provided by a thick plastic block that is located between the target chamber and the floor and contains a hole that is aligned with the hole in the concrete floor. The second nTOF LOS is located 22.1 m from TCC, above the level of the target chamber. Collimation is provided by a thick concrete wall as well as a plastic shield wall monolith. The 13-m LOS is positioned at ($\theta = 117°$, $\phi = 162°$) while the 22-m LOS is positioned at ($\theta = 79°$, $\phi = 306°$). Because of the positions of these two LOS in relation to the target chamber, the two detectors measure areal density from two distinct regions of the target. The 13-m detector measures backscattered neutrons from a section of the upper hemisphere of the target while the 22-m detector measures neutrons backscattered from a section of the lower hemisphere of the target.

III. DATA ANALYSIS

Analysis of the nTOF data is conducted via forward fit. The standard forward fit model[9] can be written as

$$V(t) = \left\{\left[50\ \Omega \times k \times s(E) \times a(E) \times \frac{\mathrm{d}N}{\mathrm{d}E_{4\pi}}\frac{\mathrm{d}E}{\mathrm{d}t}\right] \otimes \mathrm{IRF(E,\ t)}\right\} + B(t), \tag{1}$$

where $V(t)$ represents the fit to the nTOF data in units of volts, k represents a charge calibration constant in units of nC/neutron, 50 Ω represents digitizer impedance, $s(E)$ represents detector sensitivity as calculated by MCNP simulations of the xylene detector, $a(E)$ represents beamline attenuation of neutrons from the center of the OMEGA target chamber to the detector as calculated using MCNP simulations of the detector and the LOS,[3] $\frac{\mathrm{d}N}{\mathrm{d}E_{4\pi}}$ represents the total neutron spectrum exiting the ICF target into 4π, $\frac{\mathrm{d}E}{\mathrm{d}t}$ represents the relativistic Jacobian, $IRF(E,t)$ represents the energy-dependent IRF, $\otimes$ represents convolution, and $B(t)$ is a background model. For these detectors, the background is represented by an exponential decay function. This background is mainly associated with the scattering of DT neutrons on structures near the detector's LOS.

For this analysis of data from cryogenic DT implosions, the energy spectrum $\mathrm{d}N/\mathrm{d}E$ contains contributions from the DD primary, TT primary, and n(D,p)2n reactions as well as the neutrons that scatter on D and T within either the hot spot or the cold fuel shell (nD and nT). An example of the energy spectra for these components is shown in Fig. 2. Since areal densities on OMEGA are relatively low (< 350 mg/cm^2), a spectrum for multiple scatters is not currently included in this model. The DD spectrum includes parameters for an ion temperature (i.e., width), magnitude, and mean energy.[10] The TT model comes from the zero-temperature shape inferred in Ref. 11. The magnitude (or total yield) of the TT spectrum is determined using the DD:TT reactivity ratio at the inferred DD ion temperature.

The model spectra for nD and nT elastic single scatters are built such that

$$\frac{\mathrm{d}N}{\mathrm{d}E}_{\mathrm{nT+nD}} = \rho L \times Y_{\mathrm{DT}} \times \frac{f_{\mathrm{T}}\frac{\mathrm{d}\sigma_{\mathrm{nT}}}{\mathrm{d}E} + f_{\mathrm{D}}\frac{\mathrm{d}\sigma_{\mathrm{nD}}}{\mathrm{d}E}\mathrm{d}E}{f_{\mathrm{T}}m_{\mathrm{T}} + f_{\mathrm{D}}m_{\mathrm{D}}}. \tag{2}$$

Note that use of this equation assumes a point source of neutrons and an infinitesmally thin shell. The model for the n(D,p)2n spectrum comes from the cross sections inferred in Ref. 12. This spectrum also scales with areal density. The total spectrum is similarly calculated such that

$$\frac{\mathrm{d}N}{\mathrm{d}E}_{\mathrm{n(D,2n)p}} = \rho L \times Y_{\mathrm{DT}} \times \frac{f_{\mathrm{D}}\frac{\mathrm{d}\sigma_{\mathrm{n(D,2n)p}}}{\mathrm{d}E}\mathrm{d}E}{f_{\mathrm{T}}m_{\mathrm{T}} + f_{\mathrm{D}}m_{\mathrm{D}}}. \tag{3}$$

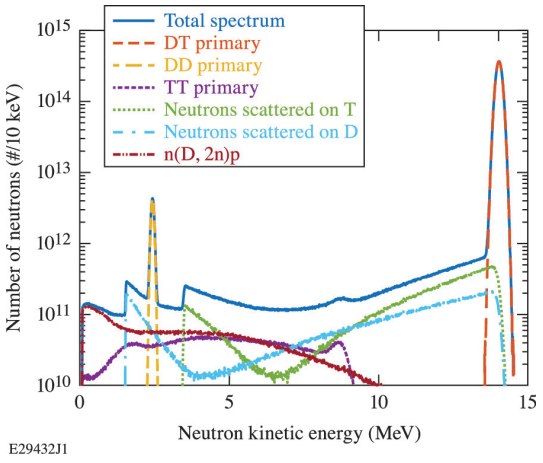

FIG. 2. *IRIS3D* neutron energy spectrum for an isobaric, symmetric areal density profile of fuel composition 50% D/50% T, 2 keV ion temperature, and shell ρR = 100 mg/cm^2.
Reproduced from Mohamed *et al.*, J. Appl. Phys., **128**, 214501 (2020), with the permission of AIP Publishing

In this model, it is assumed that the nT and nD elastic single scatters and the n(D,2n)p component all represent the same areal density. The TT, n(D,2n)p, nD single elastic scatter, and nT single elastic scatter shapes are convolved with a DT spectrum modeled at the inferred DD ion temperature in order to incorporate thermal broadening.

As previously mentioned, the analysis of nTOF data from cryogenic implosions spans a range from 1.5 to 4 MeV. Analysis over this wide range of energies allows for more accurate determination of the background. This also allows for simultaneous determination of the DD ion temperature, which directly affects the inferred background and areal density due to its effect on the magnitude of the TT spectrum. Because this analysis spans a wide range of energies, it is most accurate to use an energy-dependent IRF as detailed in Ref. 5.

The final fit has six parameters. There are four parameters related to the neutron energy spectrum: DD ion temperature, DD mean energy, DD yield, and areal density. The background is modeled as an exponential decay. The remaining 2 parameters in the forward fit are the magnitude and time decay constant for the background. The final backscatter areal density is calculated by inverting Eq. 2 such that

$$\rho L = \frac{Y_{\mathrm{nT+nD}}}{Y_{\mathrm{DT}}} \frac{f_{\mathrm{T}} m_{\mathrm{T}} + f_{\mathrm{D}} m_{\mathrm{D}}}{\int_{3.3\ \mathrm{MeV}}^{4\ \mathrm{MeV}} [f_{\mathrm{T}} \frac{\mathrm{d}\sigma_{\mathrm{nT}}}{dE} + f_{\mathrm{D}} \frac{\mathrm{d}\sigma_{\mathrm{nD}}}{dE}] \mathrm{d}E} \qquad (4)$$

where $Y_{\mathrm{nT+nD}} = \int_{3.3\ \mathrm{MeV}}^{4\ \mathrm{MeV}} \frac{\mathrm{dN}}{dE}_{\mathrm{nT\ +\ nD}} \mathrm{d}E$ and the integrated energy spectra are the best-fit spectra for the elastically scattered nD and nT neutrons. Note that this analysis focuses on the backscattered nT neutrons by integrating over 3.3 to 4 MeV.

IV. APPLICATION TO SYNTHETIC DATA

This analysis has been benchmarked using synthetic data that represent symmetric, isobaric implosions. The neutron energy spectra were generated using an ice block model in *IRIS3D*.[6] Synthetic data were then generated by propagating the simulated neutron energy spetrum through Eq. (1) with a calibration and attenuation relevant to the original xylene detector, which is located beneath the target bay at 13.4 m from TCC. The synthetic data are voltages as a function of time, which resemble experimental nTOF data. The data set involved here represents isobaric 2-keV implosions with shell areal densities (i.e., ρR values) from 50 to 250 mg/cm^2.

Note that ρL (as used in Eqs. 2-4) denotes the total (hot spot + shell) areal density as encountered by a neutron that may originate at any point within the hot spot and may scatter at any point within either the hot spot or the shell, traversing a distance that is unlikely to be equal to the shell's thickness (R).[13] In contrast, ρR denotes the areal density relevant to a radial path through the cold fuel shell alone. The analysis of nTOF data discussed here can only infer the total areal density (ρL). Similarly, *IRIS3D* models the realistic paths that neutrons may take as they scatter in a target of given hot spot and shell densities and dimensions, so the energy spectra produced by these simulations represent the ρL instead of the ρR. ρR quantities were used only to determine the appropriate input densities of the shell and hot spot in the ice block model such that the *IRIS3D* simulations represent isobaric implosions.

The forward fit to the synthetic data was carried out as detailed in the previous section, using the region of the time-resolved synthetic data corresponding to 1.5 to 4 MeV. As expected, the inferred ρL from the forward fit is different than the input shell ρR used to set up the ice block model because scattered neutrons generally traverse a distance that is not equal to the radial thickness of the shell.[13] When the energy-dependent IRF is used, the ρL inferred from the forward fit agrees with the ρL calculated directly from the *IRIS3D* energy spectra almost exactly. The relationship can be quantified using a linear fit as shown in Fig. 3. The linear fit to the ρL inferred by the forward fit to synthetic data vs. the ρL calculated directly from the *IRIS3D* energy spectra gives a slope of 1 and an intercept $<$ 1 mg/cm^2.

If either the 2.45-MeV or 3.5-MeV monoenergetic IRFs is used, $\sim$2 % inaccuracy is introduced. The comparison between the forward fit with the energy-dependent IRF and the forward fits with the two monoenergetic IRFs is summarized in Table I. This is a relatively small inaccuracy with the current analysis spanning 1.5 to 4 MeV because the only sharp features within this region are the DD signal (2.45 MeV) and the nT edge (3.5 MeV), which are relatively close in energy. For these detectors, the difference in the width of the IRF is relatively small between these two energies ($\sim$0.7-ns difference in FWHM). The inaccuracy introduced with the use of a monoenergetic

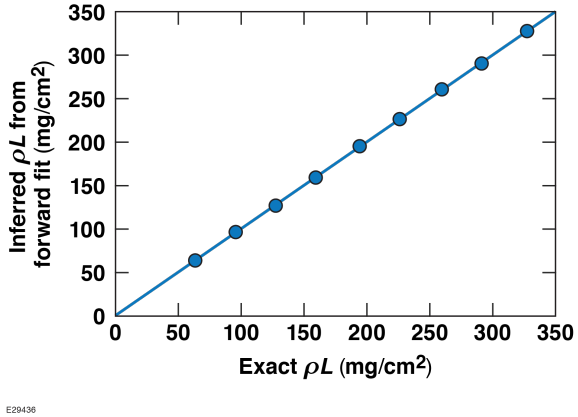

FIG. 3. Linear fit to inferred ρL from the forward fit using the energy-dependent IRF vs. ρL calculated from the raw *IRIS3D* energy spectra along with Eq. 4. Best-fit parameters from this linear fit are detailed in Table I.

IRF	Slope	Intercept
Energy-dependent	1.000 ±0.001	0.713 ±0.174
2.45-MeV monoenergetic	0.983 ±0.001	0.395 ±0.141
3.5-MeV monoenergetic	0.981 ±0.001	1.777 ±0.251

TABLE I. Best-fit parameters for a linear fit to inferred ρL from the forward fit to synthetic nTOF data vs. ρL calculated directly from the *IRIS3D* energy spectra. Three different IRF's were used in the forward fit: the energy-dependent IRF, the 2.45-MeV monoenergetic IRF, and the 3.5-MeV monoenergetic IRF. For this particular detector, the 2.45-MeV monoenergetic IRF is ∼0.7 ns larger in FWHM than the 3.5-MeV monoenergetic IRF.

IRF is expected to grow substantially if the range of the fit is extended to 9 MeV, although the exact magnitude of the effect has not yet been predicted because a more advanced energy spectrum model and a different method of determining the background will likely be required to reach this goal.

The forward fit described above is designed to be applicable for approximately symmetric implosions. Asymmetric implosions, however, can be more complicated. Since the n(D,p)2n spectrum is known to be forward-peaked while this analysis focuses on the elastically backscattered nD and nT neutrons, these spectra would not realistically scale by the same areal densities as this analysis assumes if the implosion is asymmetric.[14] Similarly, the region beneath the backscatter nT edge corresponds to forward-scattered nD neutrons, so the scaling of the nT and nD contributions at ∼3.5 MeV may change with symmetry.

It is assumed that the differences between the realistic asymmetric spectrum and the modeled symmetric spectrum will go into the "background" component of the forward fit model. It is for this reason that the background is not fixed. Changes in the "background" (i.e., a total background that originates from environmental scattering + any asymmetric contributions) have been observed in experimental data. The most obvious signature of a change in the total background is a change in the magnitude of the yield- and calibration-normalized signal in between the nT backscatter edge (3.5 MeV) and the DD primary neutrons (2.45 MeV). This area of the signal is dominated by the background from environmental scattering and the n(D,2n)p spectrum, TT primary neutrons, and forward-scattered nD neutrons. In order to further study this effect, a similar study of asymmetric synthetic data is underway.

V. EXPERIMENTALLY MEASURED VARIATIONS IN AREAL DENSITY

The current analysis using the fit for background parameters along with the symmetric nT elastic scatter, nD elastic scatter, and n(D,2n)p components has been applied to cryogenic data dating back to early 2019 (when the second nTOF LOS came online on OMEGA). An example fit to experimental data from the 13-m detector is shown in Fig. 4a. Fig. 4b shows the inferred areal densities from both detectors for a representative set of shots. With the standard beam pointing procedure and no imposed target offset, the 22-m LOS, which views part of the lower hemisphere of the target, sees an average of 20 mg/cm^2 lower than the 13-m LOS, which views part of the upper hemisphere of the target. Variations in these inferred nTOF areal densities are consistent with measured variations in ion temperature.[15]

As shown towards the right in Fig. 4b, this trend has been reversed with intentionally imposed target offsets based on measured flow velocities. In other instances, strategic target offsets based on flow velocity[15–17] have been used to minimize the areal density asymmetry. The ability to minimize or reverse the direction of the areal density asymmetry indicates that the areal density measurement responds as expected when a mode-1 perturbation is minimized or reversed in direction. These instances of minimized differences in areal densities along the two LOS correspond to shots with minimal ion temperature asymmetries as well as small flow velocities.[17]

VI. CONCLUSIONS

This work describes the analysis of nTOF data from cryogenic DT experiments with an updated analysis which uses an energy-dependent IRF and an extended range of fitting (1.5 to 4 MeV). This analysis is used to infer the areal densities for OMEGA cryogenic implosions. The energy-dependent IRF has only a small effect on the inferred areal density within the current range of fitting, but will be increasingly important as the range of the fit is extended. This method is applied as a backscat-

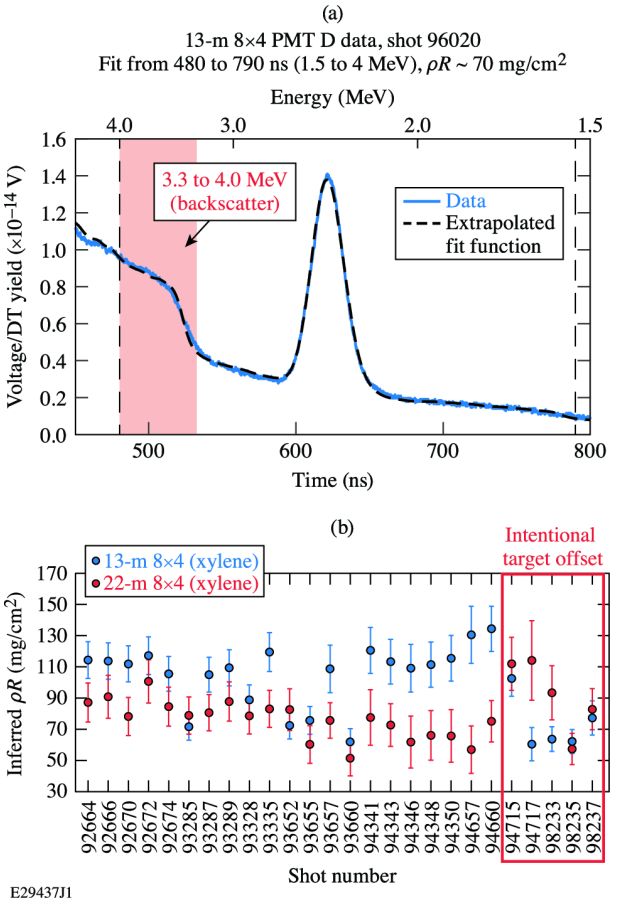

FIG. 4. (a) Example of a forward fit to experimental data for the 13-m detector. (b) Areal densities for several shots as inferred by the forward fit outlined in this work. The 22-m LOS generally infers about 20 mg/cm^2 lower than the 13-m LOS. With imposed target offsets based on the measured flow velocities, the direction of the asymmetry can be reversed or the asymmetry can be minimized.

ter areal density measurement on two detectors along two different LOS. The experimental data reveals that there is often a mode-1 asymmetry in areal density, though this can be minimized with strategically imposed target offsets based on measured flow velocities.

Future work will include further benchmarking of this analysis with asymmetric synthetic data. This will test the current handling of the background as well as the scaling of the different components [i.e., nT elastic scatters vs. nD elastic scatters vs. n(D,2n)p, which originate from different parts of the shell] and should additionally reveal any sensitivities of the current analysis to the exact shape of the nT, nD, and n(D,2n)p spectra under asymmetric conditions.

ACKNOWLEDGEMENT

This material is based upon work supported by the Department of Energy National Nuclear Security Administration under Award Number DE-NA0003856, the University of Rochester, and the New York State Energy Research and Development Authority. The support of DOE does not constitute an endorsement by DOE of the views expressed in this paper.

This report was prepared as an account of work sponsored by an agency of the U.S. Government. Neither the U.S. Government nor any agency thereof, nor any of their employees, makes any warranty, express or implied, or assumes any legal liability or responsibility for the accuracy, completeness, or usefulness of any information, apparatus, product, or process disclosed, or represents that its use would not infringe privately owned rights. Reference herein to any specific commercial product, process, or service by trade name, trademark, manufacturer, or otherwise does not necessarily constitute or imply its endorsement, recommendation, or favoring by the U.S. Government or any agency thereof. The views and opinions of authors expressed herein do not necessarily state or reflect those of the U.S. Government or any agency thereof.

DATA AVAILABILITY

The data that support the findings of this study are available from the corresponding author upon reasonable request.

[1]C. Stoeckl *et al.*, Rev. Sci. Instrum. **81**, 10D302 (2010).
[2]V. Y. Glebov *et al.*, Rev. Sci. Instrum. **85**, 11E102 (2014).
[3]C. J. Forrest *et al.*, Nucl. Instrum. Methods Phys. Res. A **888**, 169 (2018).
[4]X-5 Monte Carlo Team, Los Alamos National Laboratory, Los Alamos, NM, Report LA-UR-03-1987 (2008), .
[5]Z. L. Mohamed *et al.*, J. Appl. Phys. **128**, 214501 (2020).
[6]F. Weilacher, P. B. Radha, and C. Forrest, Phys. Plasmas **25**, 042704 (2018).
[7]R. Lauck *et al.*, IEEE Trans. Nucl. Sci. **56**, 989 (2009).
[8]V. Y. Glebov *et al.*, *Rev. Sci. Instrum.*, **75**, 3559 (2004).
[9]R. Hatarik *et al.*, J. Appl. Phys. **118**, 184502 (2015).
[10]H. Brysk, Plasma Physics **15**, 611 (1973).
[11]D. B. Sayre *et al.*, Phys. Rev. Lett. **111**, 052501 (2013).
[12]C. J. Forrest *et al.*, Phys. Rev. C **100**, 034001 (2019).
[13]G. P. Grim *et al.*, Phys. Plasmas **20**, 056320 (2013).
[14]A. J. Crilly *et al.*, Phys. Plasmas **28**, 022710 (2021).
[15]O. M. Mannion *et al.*, Rev. Sci. Instrum. **92**, 033529 (2021).
[16]O. M. Mannion *et al.*, Nucl. Instrum. Methods Phys. Res. A **964**, 163774 (2020).
[17]O. M. Mannion *et al.*, Phys. Plasmas **28**, 042701 (2021).